

# Nanoscale

Accepted Manuscript



This is an *Accepted Manuscript*, which has been through the Royal Society of Chemistry peer review process and has been accepted for publication.

*Accepted Manuscripts* are published online shortly after acceptance, before technical editing, formatting and proof reading. Using this free service, authors can make their results available to the community, in citable form, before we publish the edited article. We will replace this *Accepted Manuscript* with the edited and formatted *Advance Article* as soon as it is available.

You can find more information about *Accepted Manuscripts* in the [Information for Authors](#).

Please note that technical editing may introduce minor changes to the text and/or graphics, which may alter content. The journal's standard [Terms & Conditions](#) and the [Ethical guidelines](#) still apply. In no event shall the Royal Society of Chemistry be held responsible for any errors or omissions in this *Accepted Manuscript* or any consequences arising from the use of any information it contains.

Cite this: DOI: 10.1039/c0xx00000x

www.rsc.org/xxxxxx

ARTICLE TYPE

# Structure inherited synthesis of N-doped high-ordered mesoporous Nb<sub>2</sub>O<sub>5</sub> as robust catalysts for improved visible light photoactivity

Hui Huang,<sup>a,c</sup> Chao Wang,<sup>a</sup> Jie Huang,<sup>a,b</sup> Xiaomei Wang,<sup>a</sup> Yukou Du<sup>a</sup> and Ping Yang<sup>\*a</sup>*Received (in XXX, XXX) Xth XXXXXXXXX 20XX, Accepted Xth XXXXXXXXX 20XX*

5 DOI: 10.1039/b000000x

The high-ordered N-doped mesoporous niobium oxide (NMNb) was prepared via a facile solid state reaction method using urea as a nitrogen source. The mesoporous structure of niobium oxide (MNb) is beneficial to the N dopant effectively incorporating into the lattice of MNb, resulting in a significantly enhanced visible light response. The hydrogen generation efficiency over the optimized N-doped MNb photocatalyst was 14.8 times as high as that from N-P25 under 5 h visible light irradiation. The improved photocatalytic activity of NMNb was mainly due to that the inherited ordered mesostructure of NMNb could offer more active sites for the photocatalytic reaction, as well as accelerate the photogenerated electron-hole pairs transfer and separation.

## 15 1. Introduction

Photocatalytic splitting of water to produce hydrogen over semiconductors by sunlight is an efficient and powerful way for solar energy conversion.<sup>1,4</sup> Up to now, a large number of semiconductor-based photocatalysts, such as TiO<sub>2</sub>,<sup>5,6</sup> Nb<sub>2</sub>O<sub>5</sub>,<sup>7,8</sup> ZnO,<sup>9,10</sup> and CdS,<sup>11,12</sup> have demonstrated excellent photocatalytic activities. Among these semiconductors, niobium oxide (Nb<sub>2</sub>O<sub>5</sub>) as an n-type photocatalyst displays a lot of unique physicochemical properties, including excellent chemical and thermal stability and relatively high photocatalytic activity, which make it as a suitable photocatalyst for water splitting.<sup>13,14</sup> However, the photocatalytic activities achieved from Nb<sub>2</sub>O<sub>5</sub>-based catalysts prepared in various methods have been still modest in a view of practical application. Besides, Nb<sub>2</sub>O<sub>5</sub> can only be activated under UV-light irradiation because of its large band gap of 3.4 eV,<sup>8</sup> which limits it to use solar energy effectively. In this regard, many attempts including metal and nonmetal doping or compositing with other materials have been devoted to extend light-harvesting range.<sup>15-20</sup> Generally, various nonmetal ions (such as C, N, F, P, and S, etc.) were used to dope semiconductors, and N-doping was found to be particularly effective for visible light harvesting since the substitution of the lattice oxygen with nitrogen might narrow the band gap by mixing the N2p and O2p states.<sup>19,21</sup> To date, several research groups have synthesized N-doped Nb<sub>2</sub>O<sub>5</sub> in various methods to extend its utilization of solar energy up to the visible light region.<sup>16</sup> Some scientists also found that layered structure of niobates (HNb<sub>3</sub>O<sub>8</sub>,<sup>18</sup> KNbO<sub>3</sub><sup>21</sup>) resulted in the improved photocatalytic performance, which may be attributed to that the layered structure facilitates the photoexcited charge transfer and enhances the charge separation.

It's well known that the crystal structure and morphology of

semiconductors play significant roles on the photocatalytic activity because of charge separation and transfer of photogenerated electron-hole pairs are strongly affected by them.<sup>22,23</sup> It has been reported that Nb<sub>2</sub>O<sub>5</sub> with various morphologies like nanowires,<sup>24</sup> nanofiber<sup>25</sup> and nanoscrolls<sup>26</sup> demonstrated enhanced photocatalytic activities. More attractively, ordered mesoporous materials with continuous pore channels could short the transfer path of photogenerated carriers from bulk to the surface of the photocatalyst, and therefore decrease the electron-holes combination rate.<sup>27-30</sup> Yu's group demonstrated that the photocatalytic activity of mesoporous Nb<sub>2</sub>O<sub>5</sub> was 20 times higher than that of the bulk one without porosity.<sup>27</sup> The positive effect of mesoporosity on the photocatalytic activity was mainly ascribed to the oriented movement and efficient separation of photogenerated charges. However, to the best of our knowledge, the investigation about the N-doped mesoporous niobium oxide for photocatalytic H<sub>2</sub> evolution from water has not yet reported.

Herein, N-doped high-ordered mesoporous niobium oxide photocatalysts were prepared with a facile solid state reaction method by calcining the mixture of the mesoporous niobium oxide and urea. It was proved that the N dopant effectively incorporated in the lattice of mesoporous niobium oxide without disturbing the mesoporous structure, which significantly improved visible light photocatalytic activity. The relationship between photocatalytic activity and morphology as well as the photocatalytic reaction mechanism were also discussed. This research demonstrates a potential application of mesostructure semiconductors with controlled N doping as effective photocatalysts for solar energy conversion.

## 2. Experimental

### 2.1. Materials.

The block copolymer surfactant EO<sub>106</sub>PO<sub>70</sub>EO<sub>106</sub> (Aldrich, F127, molecular weight = 12600), niobium chloride (J&K, NbCl<sub>5</sub> ≥ 99.9%), P25 (J&K), anhydrous ethanol, anhydrous calcium chloride (CaCl<sub>2</sub>), urea, nitric acid (HNO<sub>3</sub>, 65-68%) and H<sub>2</sub>PtCl<sub>6</sub> (Alfa Aesar, > 99.9%) were purchased and used without further purification. Ultrapure water was used during the experimental process. The experiments were carried out at room temperature.

### 2.2. Synthesis of the N-Doped Mesoporous Nb<sub>2</sub>O<sub>5</sub> Photocatalysts.

The mesoporous Nb<sub>2</sub>O<sub>5</sub> photocatalyst was synthesized by self-assembly process with the aid of a structure-directing surfactant under hydrothermal conditions. Firstly, 1 g of the F127 was dissolved in 20 g of anhydrous ethanol by stirring for 10 min. To this solution, 5.5 mmol NbCl<sub>5</sub> was added with vigorous stirring for 30 min. Then, 0.5 mL of deionized water was added to the solution with further stirring for 10 min. The resulting sol was transferred to a Teflon bottle and heated at 333 K for 3 d. The aged gel samples were then washed with ethanol, dried at 313 K and calcined at 723 K for 5 h in air for the removal of the surfactant. To further perform N-doping, 1 g of the obtained mesoporous Nb<sub>2</sub>O<sub>5</sub> powder was finely milled with urea with various amounts of urea and then this combination was heated in a covered crucible at 673 K for 2 h. The yellow-colored product was crushed, washed well with nitric acid (0.1 mol·L<sup>-1</sup>) and distilled water to remove any residual alkaline species (e.g., urea and ammonia) adsorbed on the sample surface, and then dried at 343 K overnight. The final N-doped mesoporous Nb<sub>2</sub>O<sub>5</sub> products were named as NMNb-x (the x represents the weight ratio of urea/MNb, x = 1, 2 and 3). The N-doped P25 was prepared at same method and the final sample defined as N-P25.

### 2.3. Characterization.

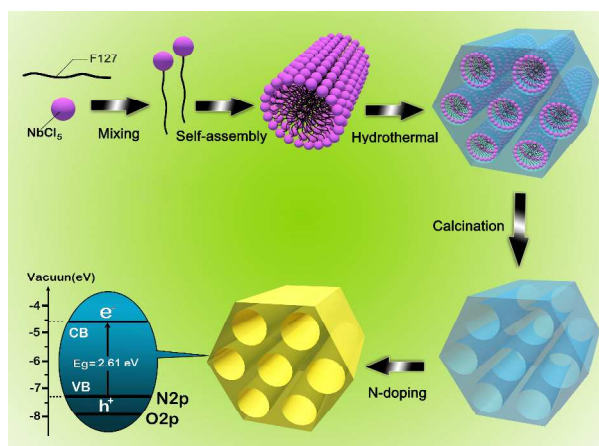
X-ray diffraction (XRD) patterns of all samples were collected in the range 10-80° (2θ) for wide angle XRD and 0.5-4° (2θ) for small angle XRD on a Philips diffract meter using Ni-filtered Cu Kα radiation. The porous properties of samples were examined by N<sub>2</sub> adsorption-desorption isotherms (BET) at 77 K. Transmission Electron Microscopy (TEM) observation was conducted on a Philips TECNAI-12 instrument. Field emission scanning electron microscopy (FESEM) measurements were taken by a Hitachi S-4700 microscope. The Energy-dispersive X-ray (EDX) analysis was performed on a KEVEX X-ray energy detector. X-ray photoelectron spectroscopy (XPS) measurements were taken by an AXIS Ultra DLD system (Kratos Analytical Inc.) using monochromatic Al Kα radiation. The samples for XPS measurements were prepared by dropping the dilute colloidal dispersion onto a silicon wafer and dried in air at room temperature. Binding energies were calculated with respect to C 1s) at 284.6 eV. Fourier transform infrared (FTIR) spectra were obtained with Thermo Scientific Nicolet 6700 instrument. Raman spectra of the samples were measured with a Jobin Yvon HR-800 spectrometer using a He-Ne laser (λ = 633 nm, spot size ~ 1 mm). UV-vis diffuse reflectance spectra (DRS) of the samples were measured on a UV-1800 SPC spectrophotometer. Photoelectrochemical measurements of the samples were carried

out on a CHI 660 B potentiostat/galvanostat electrochemical analyzer in a three-electrode system consisting of an indium tin oxide (ITO) glass covered with the sample, a platinum wire, and a Ag/AgCl electrode. The sample powder (50 mg) was ultrasonicated in 10 mL of ethanol to disperse it evenly to get a slurry. The slurry was spread onto ITO glass, whose side part was previously protected using Scotch tape. The working electrode was dried overnight under ambient conditions. The electrodes were immersed in 1 M of Na<sub>2</sub>SO<sub>4</sub> solution. The working electrode was irradiated with a GY-10 xenon lamp during the measurement. A 400 nm cut-off filter was set between the lamp and the working electrode for the visible light irradiation.

### 2.4. Measurements of Photocatalytic Activities.

The photocatalytic H<sub>2</sub> reactions were carried out in a closed gas circulation system. In our experiments, the easily oxidizable reducing reagent CH<sub>3</sub>OH was employed to evaluate the photocatalytic activity of the photocatalysts. Under stirring, the photocatalyst powder (0.02 g) was dispersed in a methanol aqueous solution (70 mL distilled H<sub>2</sub>O, 10 mL CH<sub>3</sub>OH) in an inner irradiation quartz cell. Platinum nanoparticles were deposited onto the photocatalyst surface from H<sub>2</sub>PtCl<sub>6</sub> (50 μL, 0.0396 M) methanol aqueous solution by an *in situ* photodeposition method. The loading of 0.5 wt % Pt cocatalyst was conducted by directly dissolving H<sub>2</sub>PtCl<sub>6</sub> into the above 80 mL mixed solution. Next, the system was deaerated by bubbling argon into the solution for 30 min before the reaction took place. The mixed solution was irradiated by a GY-10 xenon lamp (150 W) with cut-off filter (λ > 400 nm). All experiments were carried out at room temperature.

## 3. Results and discussion



**Scheme 1.** Schematic formation process of NMNb.

The fabrication of ordered mesoporous Nb<sub>2</sub>O<sub>5</sub> is schematically indicated in Scheme 1. Starting with hydroalcoholic solutions of NbCl<sub>5</sub> and F127, homogeneous mixture was stirred to obtain liquid-crystalline phases.<sup>31-33</sup> We speculate that the formation of the liquid-crystalline phases undergoes a direct self-assembly process of NbCl<sub>5</sub> and F127 by hydrothermal treatment. Meanwhile, the NbCl<sub>5</sub> binds to hydrophilic portion in ethylene oxide (EO) moieties along the polymer chain, leaving the hydrophobic tail (propylene oxide) folded inside. In the

hydrothermal condition, a certain temperature (333 K) and autogeneous pressure enhanced the interaction between the precursors, which led to the periodic assembly between NbCl<sub>5</sub> and the template molecules.<sup>31</sup> After removing the organic template by calcination at 723 K, the high-ordered mesoporous Nb<sub>2</sub>O<sub>5</sub> was obtained and defined as MNb. Finally, N-doped high-ordered mesoporous Nb<sub>2</sub>O<sub>5</sub> was prepared by calcining the mixture of the mesoporous niobium oxide and urea, which was defined as NMNb-x, where the x represents the weight ratio of urea/MNb, x = 1, 2 and 3.

### 3.1. Morphology and Structure Characterizations.

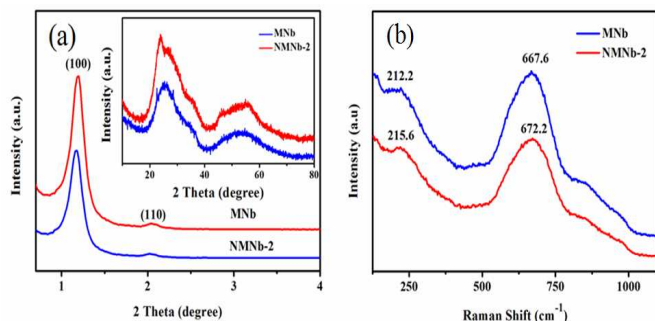


**Figure 1.** (a) Small-angle XRD and wide-angle XRD (inset) patterns of MNb and NMNb-2. (b) Raman spectra of MNb and NMNb-2.

The crystalline phase and structure of the samples were examined by powder X-ray diffraction (XRD). Small angle XRD pattern of MNb and NMNb-2 photocatalysts are shown in Figure 1 (a). Notably, two well-resolved peaks at 1.2° and 2.0°, which could be indexed as the 100 and 110 reflections, are observed for the MNb sample, corresponding to a highly ordered hexagonal structure (space group *P6mm*) and a long-range ordered mesochannels.<sup>34,35</sup> However, a decrease in peak intensities of NMNb-2 sample is found, implying that the calcination MNb with urea perturbs the mesoporous ordering of resulting sample.<sup>36</sup> Since such a decrease of the intensities is not very obvious, it is reasonable to presume that the as-prepared NMNb-2 sample still possesses a highly organized mesoporous structure.<sup>37</sup> The wide-angle XRD patterns of MNb and NMNb-2 are shown in the inset image of Figure 1 (a). The characteristic diffraction peaks at 25° and 55° show that both of the samples have formed well crystalline phase,<sup>27</sup> indicating that N-doping has a negligible effect on the crystal structure of MNb. The similar doping behavior is also observed in the N-doped mesoporous TiO<sub>2</sub> system.<sup>38</sup>

Raman spectroscopy was performed to confirm the incorporation of nitrogen into the MNb samples (Figure 1b). It can be seen that MNb and NMNb-2 samples have Raman band at 212.2 and 215.6 cm<sup>-1</sup>, respectively, which may be attributed to angle deformation modes and bridging of Nb-O-Nb bonds.<sup>39</sup> For MNb sample, the broad band centered at 667.6 cm<sup>-1</sup> can be ascribed to the main Nb-O stretching mode; however for NMNb-2, the Nb-O stretching vibration up-shifts to 672.2 cm<sup>-1</sup>, indicating the partial symmetry breaking caused by the introduction of nitrogen into MNb lattice.<sup>40</sup>

**Table 1.** Pore Structure Parameters of the MNb and NMNb-x Samples.

Sample	$S_{\text{BET}}$ (m <sup>2</sup> g <sup>-1</sup> )	$V_{\text{T}}$ (cm <sup>3</sup> g <sup>-1</sup> )	$D_{\text{BJH}}$ (nm)	N (wt %)
MNb	163	0.472	7.924	—
NMNb-1	143	0.469	7.943	1.03
NMNb-2	148	0.453	8.259	1.53
NMNb-3	136	0.443	8.023	1.71

$S_{\text{BET}}$  is the specific surface area deduced from the isotherm analysis in the relative pressure range of 0.05-0.35;  $V_{\text{T}}$  is the total pore volume at relative pressures 0.95;  $D_{\text{BJH}}$  is the average pore diameter calculated from the adsorption branch of the isotherm using the BJH method; N is the N contents analyzed by XPS.

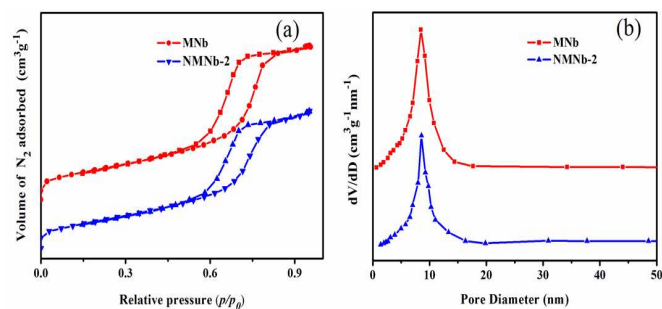


**Figure 2.** (a) N<sub>2</sub> adsorption/desorption isotherms and (b) Pore size distribution curves of the MNb and NMNb-2.

The BET surface areas and porous structures of the MNb and NMNb-2 samples were also investigated using nitrogen adsorption-desorption experiments. Both samples exhibit type IV isotherms with H2 hysteresis loop (Figure 2a), which is typical characteristics of mesoporous materials,<sup>35</sup> suggesting that the introduction of N into the crystal structure of MNb does not disturb the mesostructure.<sup>38</sup> The pore size distribution in Figure 2b obtained from adsorption curves show that both MNb and NMNb-2 samples possess an average pore diameter at ca. 8.0 nm, indicating that the pore channels are in the mesoporous region.<sup>18,38</sup> The textural properties of the samples, including BET surface area, average pore diameter, pore volume derived from N<sub>2</sub> adsorption/desorption isotherms, and pore size distributions, are summarized in Table 1. The pristine MNb is found to possess a uniform pore size of 7.9 nm with BET surface area of ca. 163 m<sup>2</sup>g<sup>-1</sup>. For the NMNb-x samples, the BET surface area decreases to ca. 140 m<sup>2</sup>g<sup>-1</sup> and the pore size ( $D_{\text{BJH}}$ ) is in ca. 8.0 nm. The decrease of pore volume of the N-doped samples is also observed but not obvious. These facts demonstrate that the mesoporous structure of the pristine MNb is inherited essentially after the incorporation of N into its crystal structure.

To provide further insight of the mesostructure of Nb<sub>2</sub>O<sub>5</sub>, the detail FESEM, TEM, HRTEM, and the electron diffraction investigations were conducted. Figure 3a presents a typical FESEM image of MNb. From the image we can see that the as-prepared mesoporous sample is composed of flake-like materials with irregular shapes (ca. 200-500 nm in width and 20-30 nm in thickness). The high-ordered hexagonal arrangement of mesopores along [110] and the alignment of cylindrical pore

channels along [001] of Nb<sub>2</sub>O<sub>5</sub> are demonstrated in the TEM images of Figure 3b-c. The hexagonal mesoporous structure with *P6mm* symmetry was further confirmed by hexagonally ordered spots in the electron diffraction patterns (inset of Fig. 3b), which is in good agreement with the results of XRD.<sup>34</sup> The TEM image of NMNb-2 is displayed in Figure 3d. The very similar image with that of MNb further reveals that NMNb-2 sample inherits the high-ordered mesoporous structure of Nb<sub>2</sub>O<sub>5</sub>. The electron diffraction pattern (inset of Figure 3d) of NMNb-2 exhibits the well-resolved diffraction spots, indicating a highly crystalline NMNb framework. In addition, the average pore diameter of both MNb and NMNb-2 obtained from TEM observation is around 8.0 nm, which is in accordance with the results calculated from N<sub>2</sub> physisorption.<sup>41</sup> Furthermore, the lattice fringes corresponding to (110) ( $d_{110} = 0.389$  nm) crystallographic planes are most frequently observed in HRTEM image (Figure 3e), disclosing the high crystallinity of the pore channels in NMNb-2. On the basis of these studies, it is reasonable to conclude that NMNb has inherited the orderliness of the mesoporous structure of MNb.

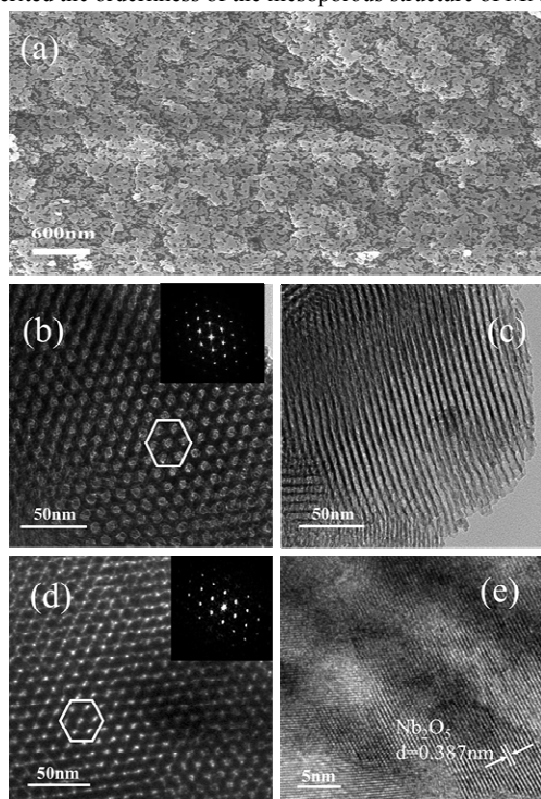


**Figure 3.** FESEM image of MNb (a); TEM images of MNb (b, c) and NMNb-2 (d) samples; HRTEM image (e) of the as-prepared NMNb-2 sample; Inset of (b and d) electron diffraction patterns.

### 3.2. XPS Analysis.

The XPS analysis is further employed to determine the composition and the surface electronic state of the as-synthesized MNb and NMNb. Figure 4a shows the survey spectrum of as-prepared samples. The signal of N can be observed from NMNb samples, indicating the successful doping of N in MNb. The nitrogen content of the samples prepared in various conditions is different. As the weight ratio of urea/MNb increases from 1 to 3, the nitrogen content increases from 1.03 to 1.71 wt % (Table 1).

The Nb 3d spectra are shown in Figure 4b. MNb presents two strong peaks located at 209.7 and 207.1 eV, corresponding to 3d<sub>5/2</sub> and 3d<sub>3/2</sub> states of Nb (V), respectively. These data agree well with previously reported data.<sup>8,42</sup> Notably, for the NMNb-2 sample, the Nb 3d<sub>3/2</sub> peak shifts to 206.7 eV. The shift of the Nb 3d<sub>3/2</sub> may be attributed to the formation of the N-Nb bond in the N-doped MNb.<sup>43,44</sup> It is known that the electron density around the Nb atom will increase when the oxygen atom in MNb is substituted by nitrogen, resulting in a decrease of the binding energy of Nb.<sup>43</sup> The O 1s XPS spectra of MNb and NMNb-2 samples are presented in Figure 4c. For MNb sample, the O 1s peak at 530.3 eV is closely related to the position of O in niobium oxide<sup>8</sup> and the slight asymmetry of the spectrum indicates that different oxygen species are present in the surface region. For NMNb-2 sample, the O 1s core level spectrum could be fitted with two peaks centered at 531.5 eV and 530.4 eV, respectively. The broad one located at the higher binding energy side may be assigned to O in Nb-O-N bond, indicating the presence of oxygen and nitrogen in the same lattice units in NMNb.<sup>43,45</sup> The N 1s XPS spectrum of NMNb is shown in Figure 4d. The peak centered at 395.7 eV is attributed to substitutional N in NMNb.<sup>21</sup> A number of studies have recently confirmed that the peak at 396 eV as  $\beta$ -N substitutionally replacing O in metal oxides lattice.<sup>21</sup> Another peak centered at 399.6 eV may be ascribed to anionic N, generally assigned as  $\gamma$ -N, incorporated in MNb in O-Nb-N linkages.<sup>45</sup> On the basis of these XPS data, we can conclude that nitrogen has already been doped successfully into lattice of MNb.

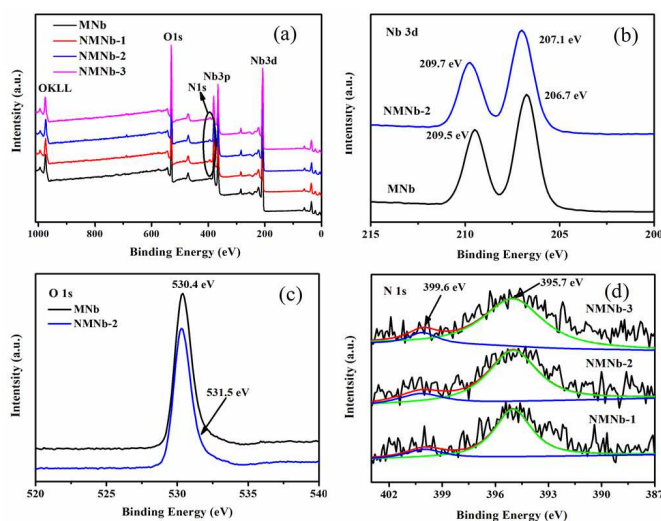


**Figure 4.** X-ray photoelectron spectra (XPS) of (a) survey spectrum of MNb and NMNb-x; (b) Nb 3d and (c) O 1s for MNb and NMNb-2; (d) N 1s for NMNb-x samples.

### 3.3. Optical and Photoelectrochemical Properties of the Samples.

The optical properties of MNb and NMNb-x samples were investigated by UV-visible diffuse reflectance spectroscopy, and the results were depicted in Figure 5. The absorption edge of MNb is ca. at 400 nm, while the absorption edge of the NMNb samples red-shifts obviously. With the increasing of N content in the sample, the onset of the absorption shifts smoothly to longer wavelengths and the absorption intensity augments. The

improved absorption of the N-doped samples is ascribed to that the additional electronic states formed by N2p band are located above the valence band derived mainly from O2p orbitals, which is similar to the case of N-doped TiO<sub>2</sub>.<sup>19,43</sup> The theory of interband optical absorption reveals that the optical absorption coefficient ( $\alpha$ ) varies with the photon energy ( $h\nu$ ) according to the expression  $(\alpha h\nu)^n = A(h\nu - E_g)$ , where  $A$  and  $E_g$  are constant and the band gap energy, respectively, and  $n$  is a number which characterizes the transition process, which takes the value 2 for a directly allowed transition. The calculated band gap energy ( $E_g$ ) for the MNb and N-doped samples is about 3.12 (MNb), 2.98 (NMNb-1), 2.61 (NMNb-2) and 2.82 (NMNb-3) eV. The NMNb-2 sample with a band gap of 2.61 eV indicates that it is capable of capturing the light shorter than 475 nm. The observation of higher N-doping resulting in the band gap widening is consistent with the report of Pillai's group, which could be attributed to the result of excessive crystallite growth on increasing N concentration.<sup>43</sup>

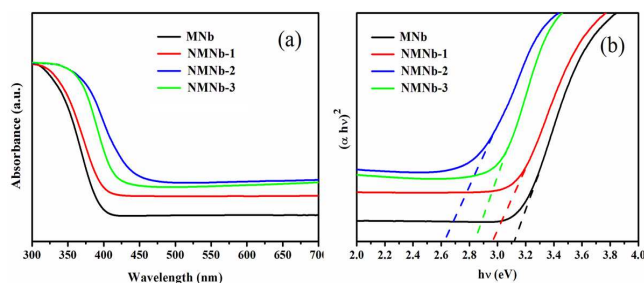


**Figure 5.** The UV-vis diffuse reflectance spectra of MNb and NMNb-x.

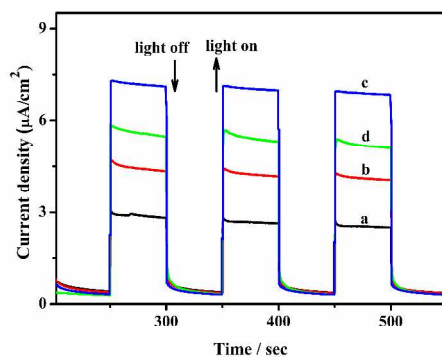


**Figure 6.** Photocurrents of (a) MNb, (b) NMNb-1, (c) NMNb-2 and (d) NMNb-3 under visible light irradiation ( $\lambda > 420$  nm) at a bias potential of 1.2 V vs Ag/AgCl. The illumination from a 150 W xenon lamp was interrupted every 50 s.

The results of photoelectrochemical experiments performed under visible light illumination are shown in Figure 6. The photocurrent density generated by MNb was  $3 \mu\text{A}\cdot\text{cm}^{-2}$ , whereas the photocurrent densities for the NMNb-x samples increased obviously. The photocurrent densities for NMNb-1, NMNb-2 and NMNb-3 reached to  $4.5$ ,  $7.5$ , and  $5.8 \mu\text{A}\cdot\text{cm}^{-2}$ , respectively. The maximum photocurrent density produced by NMNb-2 electrode is ca. 2.5 times as higher as that of MNb. The fact of the photocurrent enhancement suggests that N-doped MNb with a

narrower band gap may harvest visible-light more efficiently. In addition, the incorporation of N in MNb may also help to eliminate some oxygen vacancies presented in the lattice of MNb, leading to reduced trap state distributions and enhanced the separation efficiency of the photogenerated carriers.<sup>46</sup> However, when the N concentration in MNb is above the optimized value, the photocurrent density decreases, which may be due to that excessive N acts as the recombination centers for photogenerated electron-holes, thereby reducing the photocurrent density.<sup>47</sup>

### 3.4. Photocatalytic Activity for H<sub>2</sub> Evolution and Tentative Mechanism of Photocatalytic Reaction.

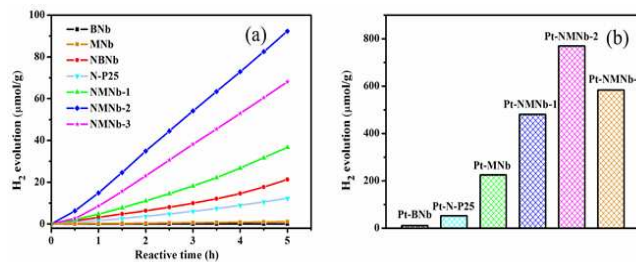


**Figure 7.** (a) Photocatalytic hydrogen production rates over a series of Nb under visible light ( $\lambda > 400$  nm) irradiation for 5 h. Reaction conditions:  $m_{\text{catalyst}} = 20$  mg,  $\text{pH} = 7$ ,  $T = 298$  K, light source: 150 W Xe lamp with cut-off filter ( $\lambda > 400$  nm) and (b) Effect of the Pt loading on the amount of H<sub>2</sub> evolution under visible light irradiation for 5 h. Reaction conditions:  $m_{\text{catalyst}} = 20$  mg,  $[\text{Pt}] = 0.5$  wt %,  $\text{pH} = 7$ ,  $T = 298$  K, light source: 150 W Xe lamp with cut-off filter ( $\lambda > 400$  nm).

The photocatalytic results of the different samples for photocatalytic H<sub>2</sub> evolution are shown in Figure 7a. Under visible light irradiation, almost no H<sub>2</sub> was detected when bulk Nb<sub>2</sub>O<sub>5</sub> (BNb) or MNb was used as a photocatalyst. However, for N-doped BNb (NBNb), the amount of H<sub>2</sub> evolution was  $21.3 \mu\text{mol}\cdot\text{g}^{-1}$  under 5 h visible-light irradiation, which could be mainly ascribed to that N doping BNb narrowed the band gap and shifted the absorption edge toward visible light region, thereby enhanced the visible-light photocatalytic activity.<sup>46</sup> For the N-doped mesoporous samples, NMNBs display much higher hydrogen evolution activity. Under 5 h visible light irradiation, the amount of H<sub>2</sub> evolution from NMNb-2 is  $92.3 \mu\text{mol}\cdot\text{g}^{-1}$ , which is 4.3 times as high as that of NBNb ( $21.3 \mu\text{mol}\cdot\text{g}^{-1}$ ) and 7.5 times as that of N-P25 ( $12.2 \mu\text{mol}\cdot\text{g}^{-1}$ ). The enhanced photocatalytic activity of the NMNB samples might be attributable to that N-doped MNb with a narrower band gap may utilize visible light efficiently, and that the well inherited mesoporous structure could offer a great number of active sites for the photocatalytic reaction, as well as a short distance for photoexcited charge carrier transfer, thus, lowering the charge recombination.<sup>27,38</sup>

The effect of the Pt loading on the amount of H<sub>2</sub> evolution is shown in Figure 7b. After being irradiated under visible-light for 5 h, the amount of H<sub>2</sub> evolved from platinized BNb photocatalyst was  $11.3 \mu\text{mol}\cdot\text{g}^{-1}$ , while the amount of hydrogen produced from platinized MNb was  $224.9 \mu\text{mol}\cdot\text{g}^{-1}$ . However, platinized NMNBs showed remarkable enhancement in photocatalytic activity for hydrogen evolution. The amount of hydrogen evolved from

platinized NMNb-1, NMNb-2, and NMNb-3 was 480.5, 770.0, and 583.8  $\mu\text{mol}\cdot\text{g}^{-1}$ , respectively. In particular, the highest  $\text{H}_2$  evolution amount from platinized NMNb-2 was found to be ca. 3.4 and 14.8 times as high as that of platinized MNb and N-P25 (52.1  $\mu\text{mol}\cdot\text{g}^{-1}$ ), respectively. Such enhancement of  $\text{H}_2$  evolution activity for the platinized NMNb photocatalysts was due to that platinum acts as a cocatalyst able to capture electrons and to reduce electrochemical proton reduction overpotential, thus, increasing the separation efficiency of photogenerated carriers.<sup>27,48,49</sup> Meanwhile, the well inherited mesostructure of NMNbs provides large surface area for anchoring Pt nanoparticles, consequently, the platinized NMNb catalysts demonstrated markedly promoted photocatalytic activity.

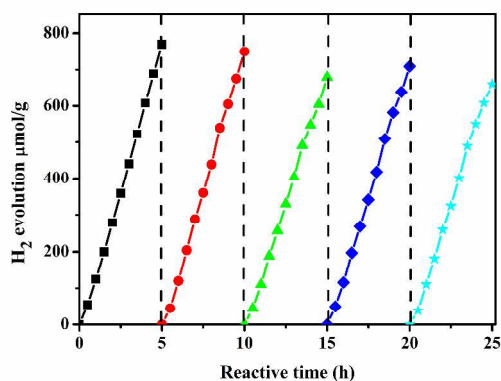
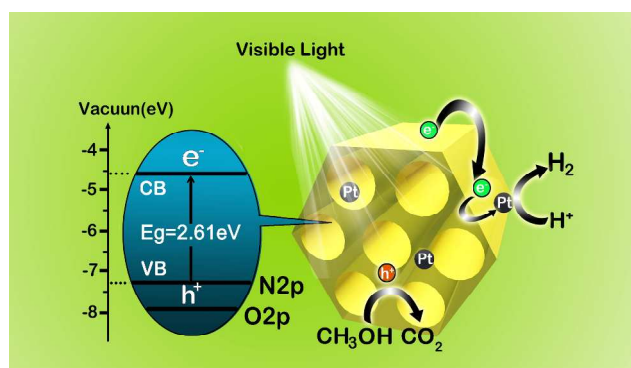


**Figure 8.** Recycle study of the photocatalyst NMNb-2.

15

The stability of NMNb-2 for  $\text{H}_2$  evolution under visible light irradiation is presented in Figure 8. It shows that the hydrogen evolution yield remains basically unchanged after 25 h visible-light irradiation, indicating sufficient stability of NMNb-2 for photocatalytic hydrogen evolution.

20



**Scheme 2.** Schematic photoexcited electron transfer and hydrogen evolution over the NMNb photocatalyst under visible light irradiation.

25

On the basis of the above results, a tentative mechanism of the photocatalytic reaction is proposed as illustrated in Scheme 2. Under the irradiation of visible light, the electrons ( $e^-$ ) were excited from valence band to the conduction band of NMNb, then migrated to the Pt nanoparticles deposited on the surface of NMNb for proton reduction to produce hydrogen. The holes in the valence band of NMNb transferred to oxidize  $\text{CH}_3\text{OH}$  to  $\text{CO}_2$ . Because the high-ordered mesoporous structure of NMNb

30

provides a short diffusion pathway for photoexcited electron-holes transfer<sup>28,29</sup> and the formed N-doping level in NMNb narrows the band gap of the semiconductor by mixing the N2p and O2p states, the NMNb catalysts demonstrate remarkable enhanced visible light active for water reduction to produce hydrogen.<sup>19,43</sup> Our research suggests that the N-doped mesoporous niobium oxide is a promising candidate as a novel solar-active photocatalyst for photocatalytic hydrogen evolution.

#### 4. Conclusions

In summary, high-ordered N-doped mesoporous  $\text{Nb}_2\text{O}_5$  has been successfully prepared via a facile solid state reaction method. The resultant NMNb-2 sample exhibited a significantly enhanced visible light response, corresponding to a reduced band gap of 2.61 eV by mixing the N2p and O2p orbital. Benefiting from the positive N-doping effect, large surface area and the inherited high-ordered mesoporous structure, the hydrogen production yield over NMNb-2 is up to 770.0  $\mu\text{mol}\cdot\text{g}^{-1}$  under 5 h visible light irradiation. This study suggests that fabricating ordered mesoporous semiconductor with appropriate N-doping is a feasible and simple approach for solar energy conversion.

45

50

## Acknowledgements

The authors gratefully acknowledge financial support of this research by the National Natural Science Foundation of China (21373143 and 51273141), the Priority Academic Program Development of Jiangsu Higher Education Institutions (PAPD), and Qing Lan Project of Jiangsu Province.

## Notes and references

<sup>a</sup> College of Chemistry, Chemical Engineering and Materials Science, Soochow University, Suzhou 215123, China. Fax: +86-512-6588 0089;

10 Tel.: +86-512-6588 0361; E-mail address: pyang@suda.edu.cn.

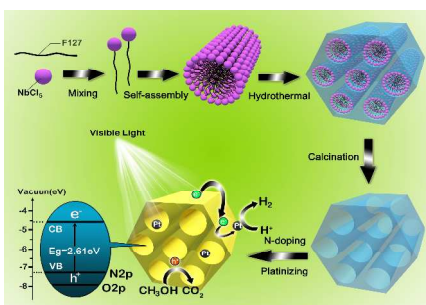
<sup>b</sup> Suzhou Institute of Nano-tech and Nano-bionics, Chinese Academy of Sciences, Suzhou 215123, China

<sup>c</sup> Department of Chemistry, Nantong Vocational College, Nantong 226007, China

15 †Electronic Supplementary Information (ESI) available. See DOI: 10.1039/b000000x/

1. A. Kudo and Y. Miseki, *Chem. Soc. Rev.*, 2009, **38**, 253-278.
2. X. B. Chen, S. H. Shen, L. J. Guo and S. S. Mao, *Chem. Rev.*, 2010, **110**, 6503-6570.
3. K. Maeda and K. Domen, *J. Phys. Chem. Lett.*, 2010, **1**, 2655-2661.
4. J. Zhang, P. W. Du, J. Schneider, P. Jarosz and R. Eisenberg, *J. Am. Chem. Soc.*, 2007, **129**, 7726-7727.
5. S. U. M. Khan, M. Al-Shahry and W. B. Ingler, *Science*, 2002, **297**, 2243-2245.
6. N. S. Chaudhari, S. S. Warule, S. A. Dhanmane, M. V. Kulkarni, M. Valantb and B. B. Kale, *Nanoscale*, 2013, **5**, 9383-9390.
7. R. Ghosh, M. K. Brennaman, T. Uher, M. R. Ok, E. T. Samulski, L. E. McNeil, T. J. Meyer and R. Lopez, *ACS Appl. Mater. Interfaces*, 2011, **3**, 3929-3935.
8. S. X. Ge, H. M. Jia, H. X. Zhao, Z. Zheng and L. Z. Zhang, *J. Mater. Chem.*, 2010, **20**, 3052-3058.
9. W. L. Ong, S. Natarajan, B. Kloostrab and G. W. Ho, *Nanoscale*, 2013, **5**, 5568-5575.
10. A. Wolcott, W. A. Smith, T. R. Kuykendall, Y. P. Zhao and J. Z. Zhang, *Adv. Funct. Mater.*, 2009, **19**, 1849-1856.
11. Q. Li, H. Meng, P. Zhou, Y. Q. Zheng, J. Wang, J. G. Yu and J. R. Gong, *ACS Catal.*, 2013, **3**, 882-889.
12. T. H. Yu, W. Y. Cheng, K. J. Chao and S. Y. Lu, *Nanoscale*, 2013, **5**, 7356-7360.
13. H. Y. Lin, H. C. Huang and W. L. Wang, *Micropor. Mesopor. Mat.*, 2008, **115**, 568-575.
14. A. Esteves, L. Oliveira, T. Ramalho, M. Goncalves, A. Anastacio and H. Carvalho, *Catal. Commun.*, 2008, **10**, 330-332.
15. H. Y. Lin, H. C. Yang and W. L. Wang, *Catal. Today*, 2011, **174**, 106-113.
16. R. Ullah, H. Sun, H. M. Ang, M. O. Tadé and S. B. Wang, *Ind. Eng. Chem. Res.*, 2013, **52**, 3320-3328.
17. X. K. Li, N. Kikugawa and J. H. Ye, *Adv. Mater.*, 2008, **20**, 3816-3819.
18. A. Mukherji, B. Seger, G. Q. Lu and L. Z. Wang, *ACS Nano*, 2011, **5**, 3483-3492.
19. R. Asahi, T. Morikawa, T. Ohwaki, K. Aoki and Y. Taga, *Science*, 2001, **293**, 269.
20. X. Wang, G. Chen, C. Zhou, Y. G. Yu and G. Wang, *Eur. J. Inorg. Chem.*, 2012, **2012**, 1742-1749.
21. R. W. Wang, Y. F. Zhu, Y. F. Qiu, C. F. Leung, J. He, G. J. Liu and T. C. Lau, *Chem. Eng. J.*, 2013, **226**, 123-130.
22. M. C. Liu, D. W. Jing, Z. H. Zhou and L. J. Guo, *Nat. Commun.*, 2013, **4**, 2278.
23. L. Pan, J. J. Zou, S. B. Wang, X. Y. Liu, X. W. Zhang and L. Wang, *ACS Appl. Mater. Interfaces*, 2012, **4**, 1650-1655.
24. K. Okumura, T. Tomiyama, S. Shirakawa, S. Ishida, T. Sanada and M. Arao, M. Niwa, *J. Mater. Chem.*, 2011, **21**, 229-235.
25. K. Maeda, M. Eguchi, W. J. Youngblood and T. E. Mallouk, *Chem. Mater.*, 2008, **20**, 6770-6778.
26. H. Shima, M. Tanaka, H. Imai, T. Yokoi, T. Tatsumi and J. N. Kondo, *J. Phys. Chem. C*, 2009, **113**, 21693-21699.
27. X. Y. Chen, T. Yu, X. X. Fan, H. T. Zhang, Z. S. Li, J. H. Ye and Z. G. Zou, *Appl. Surf. Sci.*, 2007, **253**, 8500-8506.
28. J. N. Kondo, M. Uchida, K. Nakajima, L. Daling, M. Hara and K. Domen, *Chem. Mater.*, 2004, **16**, 4304-4310.
29. Y. Li, Z. Y. Fu and B. L. Su, *Adv. Funct. Mater.*, 2012, **22**, 4634-4667.
30. J. N. Kondo, M. Uchida, K. Nakajima, L. Daling, M. Hara and K. Domen, *Chem. Mater.*, 2004, **16**, 4304-4310.
31. D. Y. Zhao, J. L. Feng, Q. S. Huo, N. Melosh, G. H. Fredrickson, B. F. Chmelka and G. D. Stucky, *Science*, 1998, **279**, 548-552.
32. C. J. Brinker, Y. F. Lu, A. Sellinger and H. Y. Fan, *Adv. Mater.*, 1999, **11**, 579-585.
33. L. Y. Song, D. Feng, N. J. Fredin, K. G. Yager, R. L. Jones, Q. Y. Wu, D. Y. Zhao and B. D. Vogt, *ACS Nano*, 2010, **4**, 189-198.
34. T. Katou, D. L. Lu, J. N. Kondo and K. Domen, *J. Mater. Chem.*, 2002, **12**, 1480-1483.
35. B. Lee, D. L. Lu, J. N. Kondo and K. Domen, *J. Am. Chem. Soc.*, 2002, **124**, 11256-11257.
36. S. H. Liu and J. R. Wu, *Int. J. Hydrogen. Energ.*, 2011, **36**, 87-93.
37. H. Y. Hao and J. L. Zhang, *Micropor. Mesopor. Mat.*, 2009, **121**, 52-57.
38. S. H. Liu and H. R. Syu, *Appl. Energ.*, 2012, **100**, 148-154.
39. M. P. F. Graça, A. Meireles, C. Nico and M. A. Valente, *J. Alloy. Compd.*, 2013, **553**, 177-182.
40. J. W. Wang, W. Zhu, Y. Q. Zhang and S. X. Liu, *J. Phys. Chem. C*, 2006, **111**, 1010-1014.
41. J. G. Wang, Z. F. Bian, J. Zhu and H. X. Li, *J. Mater. Chem. A*, 2013, **1**, 1296-1302.
42. S. Furukawa, T. Shishido, K. Teramura and T. Tanaka, *ACS Catal.*, 2011, **2**, 175-179.
43. V. Etacheri, M. K. Seery, S. J. Hinder and S. C. Pillai, *Chem. Mater.*, 2010, **22**, 3843-3853.
44. P. Madhusudan, J. Ran, J. Zhang, J. G. Yu and G. Liu, *Appl. Catal. B: Environ.*, 2011, **110**, 286-295.
45. M. Sathish, B. Viswanathan, R. P. Viswanath and C. S. Gopinath, *Chem. Mater.*, 2005, **17**, 6349-6353.
46. Y. K. Lai, J. Y. Huang, H. F. Zhang, V. P. Subramaniam, Y. X. Tang, D. G. Gong, L. Sundar, L. Sun, Z. Chen and C. J. Lin, *J. Hazard. Mater.*, 2010, **184**, 855-863.
47. Y. Binyu, M. L. Woon and Y. Jun, *Nanotechnology*, 2013, **24**, 335705.
48. Q. Li, B. D. Guo, J. G. Yu, J. R. Ran, B. H. Zhang, H. J. Yan and J. R. Gong, *J. Am. Chem. Soc.*, 2011, **133**, 10878-10884.
49. P. D. Tran, S. K. Batabyal, S. S. Pramana, J. Barber, L. H. Wong and S. C. J. Loo, *Nanoscale*, 2012, **4**, 3875-3878.

## Graphical Abstract



Structure inherited synthesis of N-doped high-ordered mesoporous Nb<sub>2</sub>O<sub>5</sub> as efficient and stable visible-light-driven photocatalyst for hydrogen evolution